Supplementary Information

Copper-transporting P-type ATPases use a unique ion-release pathway

Magnus Andersson[1*#], Daniel Mattle[2*], Oleg Sitsel[2], Anna Marie Nielsen[2], Stephen H. White[1], Poul Nissen[2] & Pontus Gourdon[2]

[1] Department of Physiology and Biophysics, University of California at Irvine, Irvine, CA 92697-4560, USA

[2] Centre for Membrane Pumps in Cells and Disease - PUMPKIN, Danish National Research Foundation, Aarhus University, Department of Molecular Biology and Genetics, Gustav Wieds Vej 10C, DK-8000 Aarhus C, Denmark

[*] contributed equally

[#] Magnus Andersson's present address is Science for Life Laboratory, Department of Theoretical Physics, Swedish e-Science Research Center, KTH Royal Institute of Technology, SE-171 21 Solna, Sweden

Figures – Supplementary Figure 1

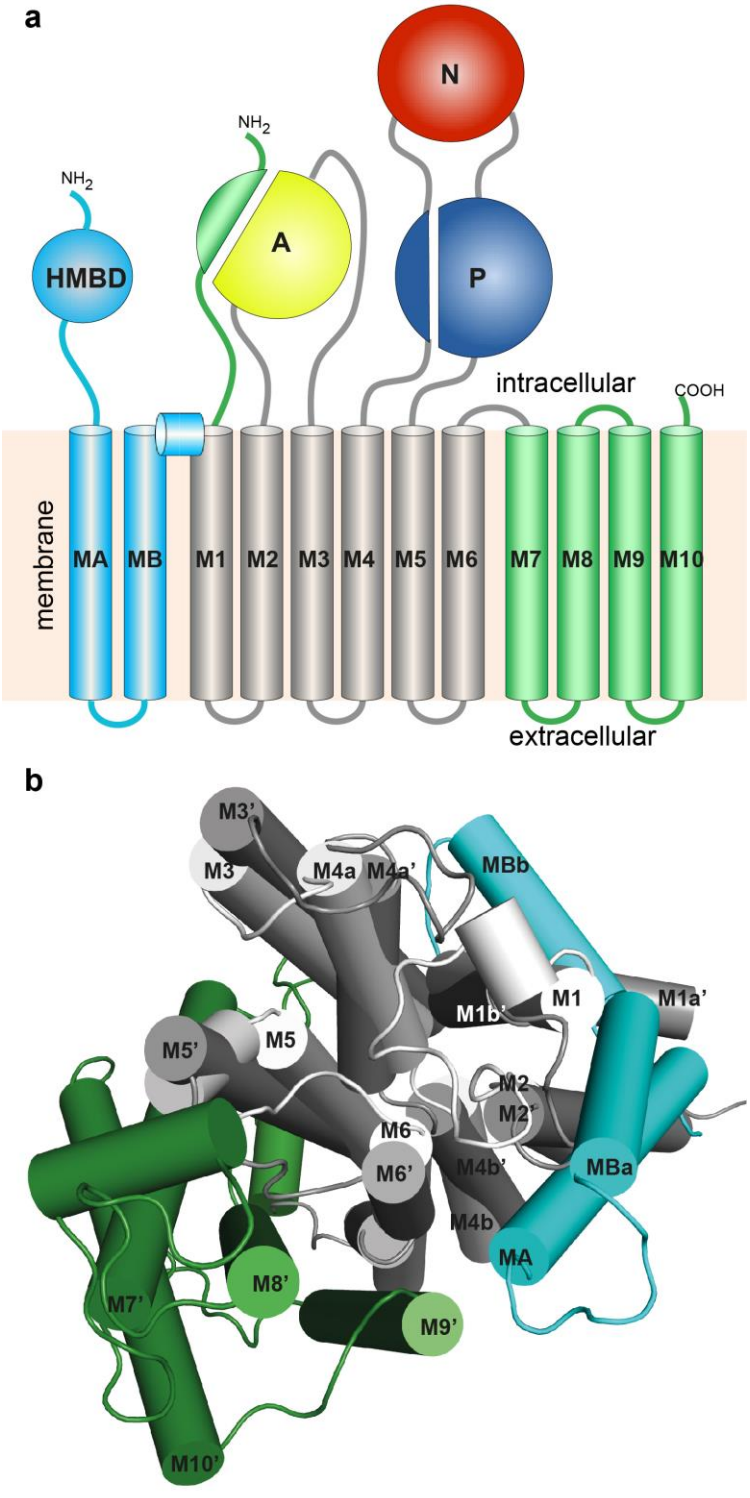

Supplementary Figure 1. **Major differences between CopA and SERCA.** Features unique to CopA and SERCA colored in cyan and green, respectively. **a,** The P-type ATPases topology with the domains colored as in Fig. 1a. **b,** View from the extra-cellular side of the helical organization of the E2P states of the two proteins. The common transmembrane helices M1-M6 (apostrophes for SERCA) were aligned (LpCopA residues 147-210, 332-404 and 664-736 on residues 49-124, 247-330 and 751-816 in SERCA, pdb-id: 3B9B[1]) using super in PYMOL (www.pymol.org).

Figures – Supplementary Figure 2

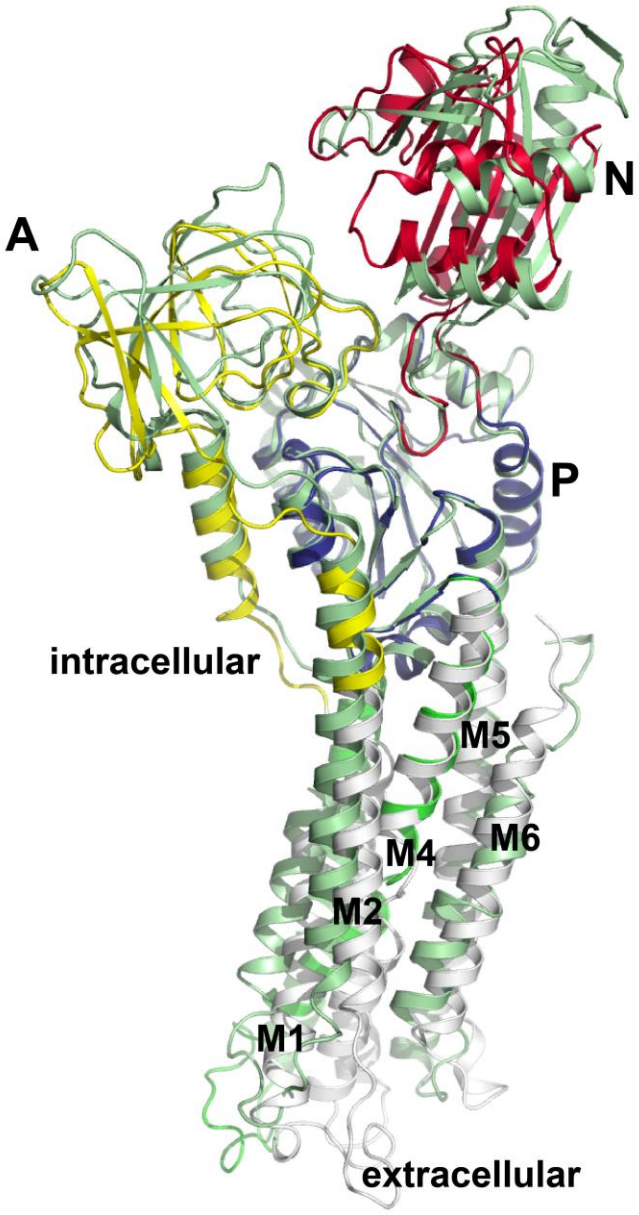

Supplementary Figure 2. Overview of the domain arrangements in the E2P states of LpCopA and SERCA. LpCopA is colored as in Fig. 1a and SERCA (pdb-id: 3B9B[1]) is shown in green. Superimpositions were made of the intracellular domains using super in PYMOL (www.pymol.org) with LpCopA residues 225-332 and 404-664 on residues 125-239 and 344-750 of SERCA). Transmembrane helices MA and MB (LpCopA) and M7-M10 (SERCA) as well as SERCA insertions (residues 1-59, 370-408, 421-439, 453-478 567-591) have been removed for clarity.

Figures – Supplementary Figure 3

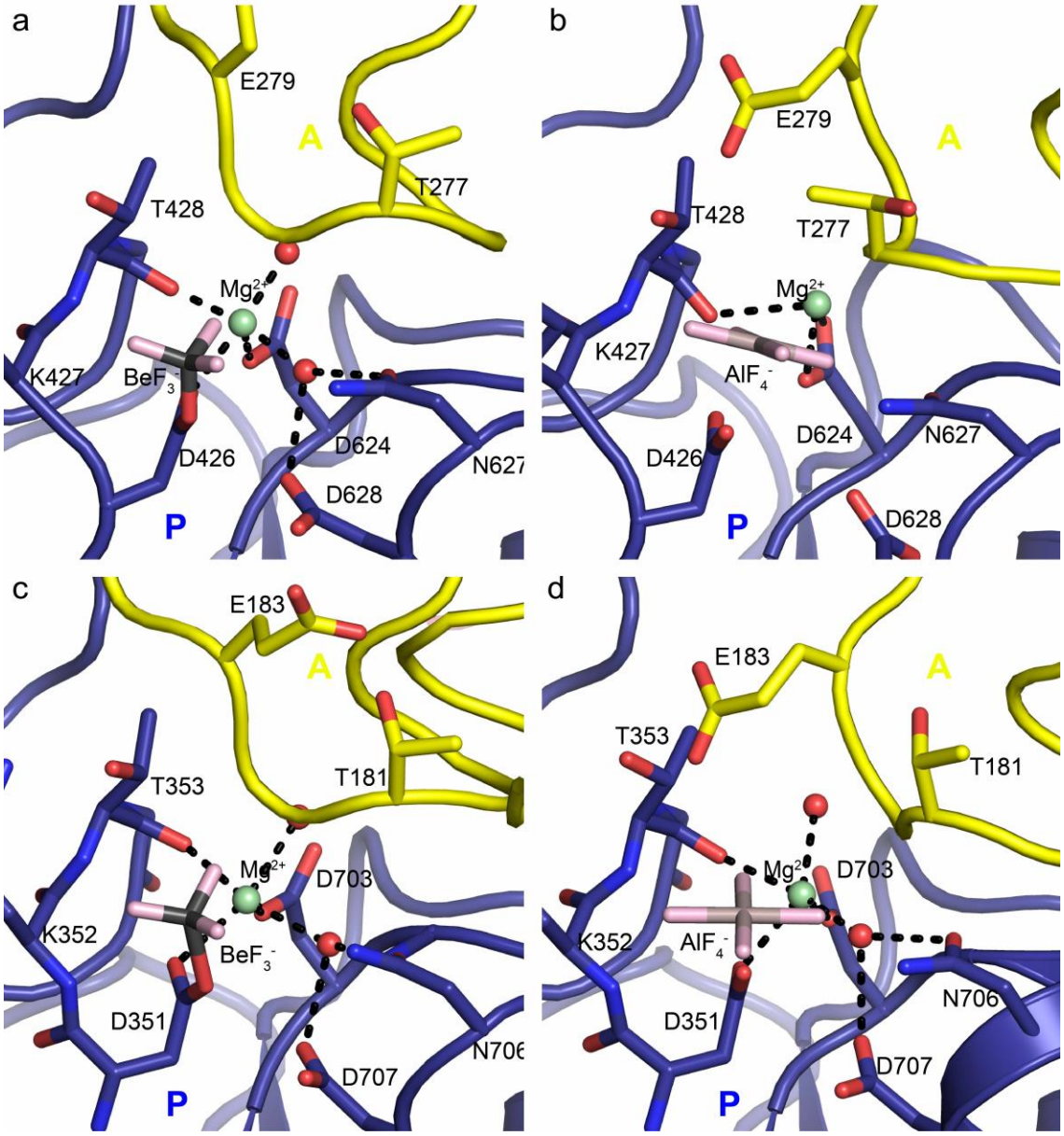

Supplementary Figure 3. Close-up view of the phosphorylation site of LpCopA and SERCA. The panels show the region around the phosphorylation site at the interface between the A-, P-, and N-domains, and compare the E2P phosphoenzyme (BeF_3^- complex) to the transition state of dephosphorylation (AlF_4^- complex). The domains are indicated by colors as in Fig. 1a and the catalytic aspartate (Asp426 in the DKTGT

motif), Lys427, Thr428, Asp624, Asn627 and Asp628 (in the P-domain) as well as Thr277 and Glu279 (of the TGE motif in the A-domain, associated with dephosphorylation) are shown as sticks. **a,** The E2P state presented in this work, determined as a complex with BeF_3^- (Be in black, F in pink) and the Mg^{2+} ion (green) associated with Asp426. **b,** The subsequent (forward reaction) E2.P_i conformation with AlF_4^- (Al in brown, F in pink) and the Mg^{2+} ion (green) associated with Asp426 (pdb-id: 3RFU[2]). Note the significant shift in the position of the A-domain relative to the P-domain between the two functional conformations. **c,** Equivalent view as in panel a for the E2P state of SERCA (pdb-id: 3B9B[1]). **d,** Equivalent view as in panel b for the E2.P_i state of SERCA (pdb-id: 3B9R[1]).

Figures – Supplementary Figure 4

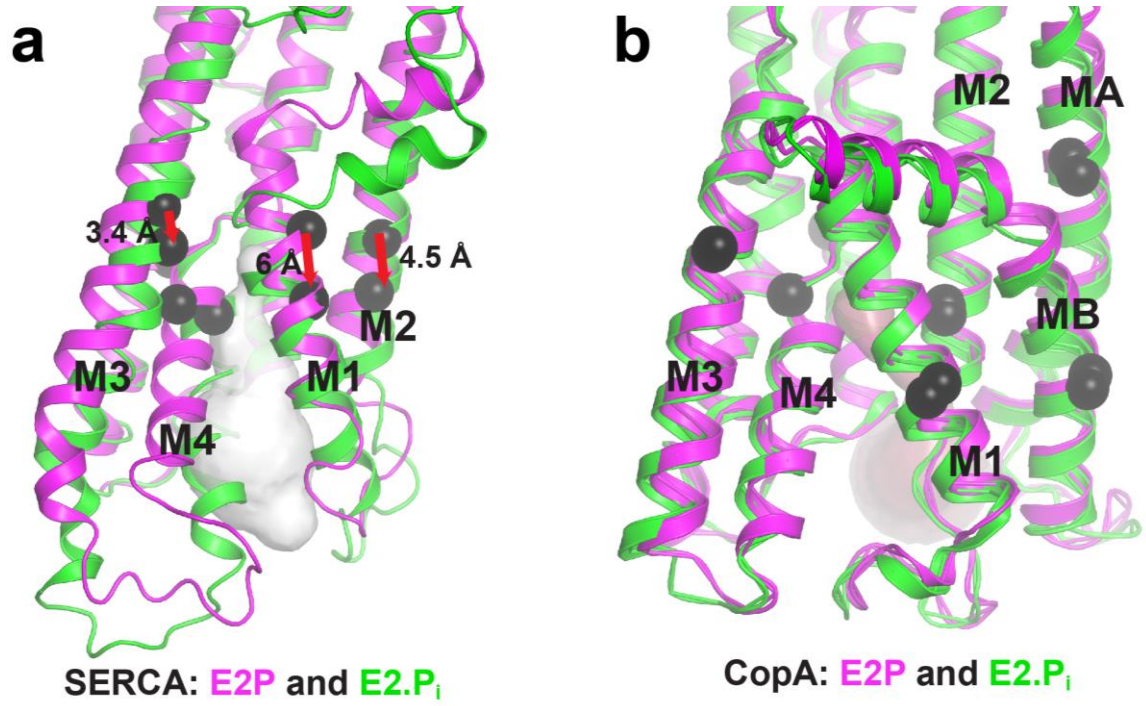

Supplementary Figure 4. The transmembrane domains of the E2P and E2.P$_i$ structures of LpCopA and SERCA. Significant shifts of helices M1-M2 and M3-M4 change SERCA from open in the E2P state (pdb-id: 3B9B[1]) to occluded with bound protons in the [H_2]E2.P$_i$ state (pdb-id: 3B9R[1]) while in LpCopA the domain remains nearly constant. Superimpositions were made using super in PYMOL (www.pymol.org). Alternative views are also shown in Fig. 3a,b. **a,** The open E2P (purple) and occluded E2.P$_i$ (green) states of SERCA aligned on M5 and M6 (residues 740-781 and 788-810). Black spheres indicate the movements of one Cα atom in each helix. The release pathway, formed between M1-M2, M3-M4 and M5-M6, is shown in white. Transmembrane helices M7-M10 have been removed for clarity. **b,** Equivalent view of the open E2P (purple) and E2.P$_i$ (green) (pdb-id: 3RFU[2]) states of CopA aligned on M5 and M6 (residues 664-697 and 712-736), colored as in a and with MA and MB in cyan. The release pathway, formed between MA, M2 and M6 is shown in purple.

Figures – Supplementary Figure 5

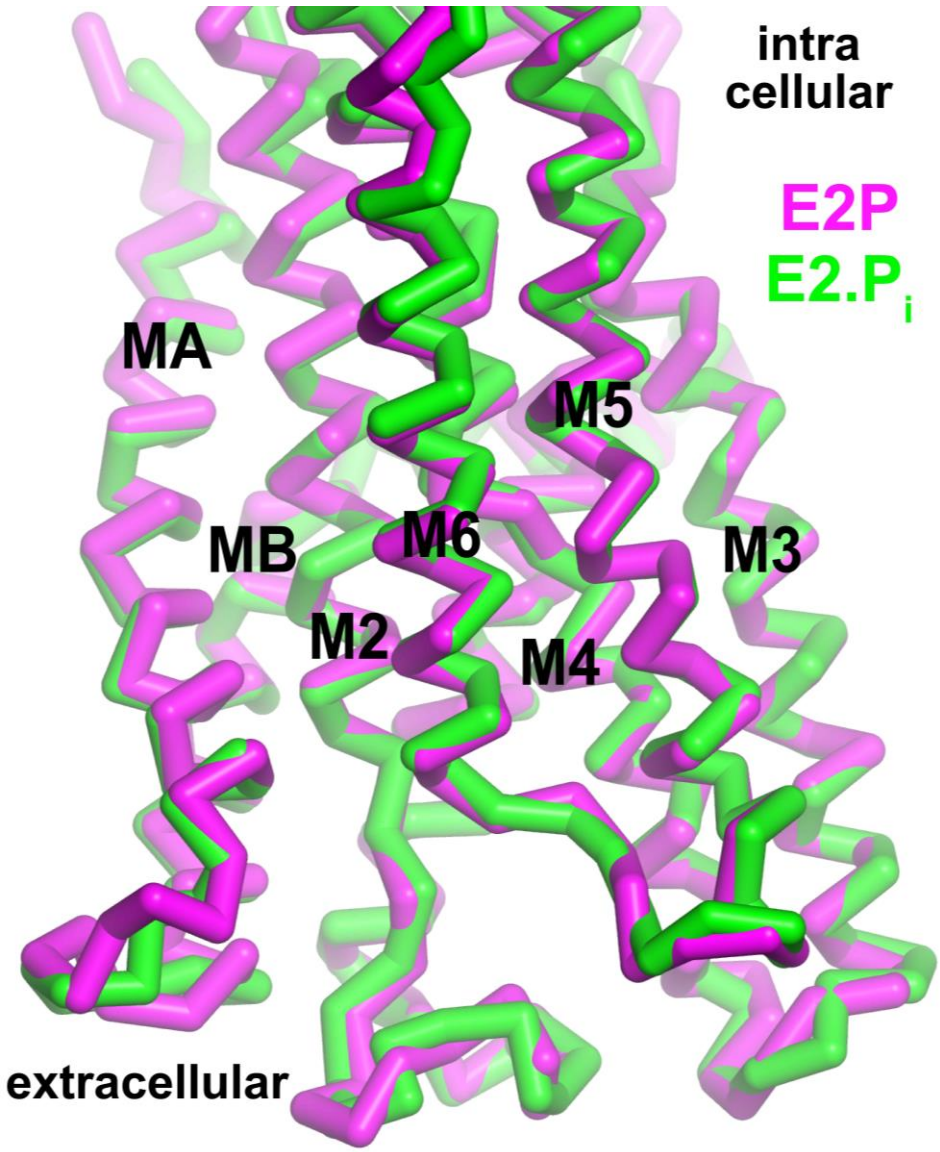

Supplementary Figure 5. The similar transmembrane domains of the E2P and E2.P$_i$ states of LpCopA. The E2P and E2.P$_i$ (pdb-id: 3RFU[2]) states are shown in purple and green, respectively. Superimpositions of these domains were made using super in PYMOL (www.pymol.org) using residues 74–203, 335–390 and 679–730.

Figures – Supplementary Figure 6

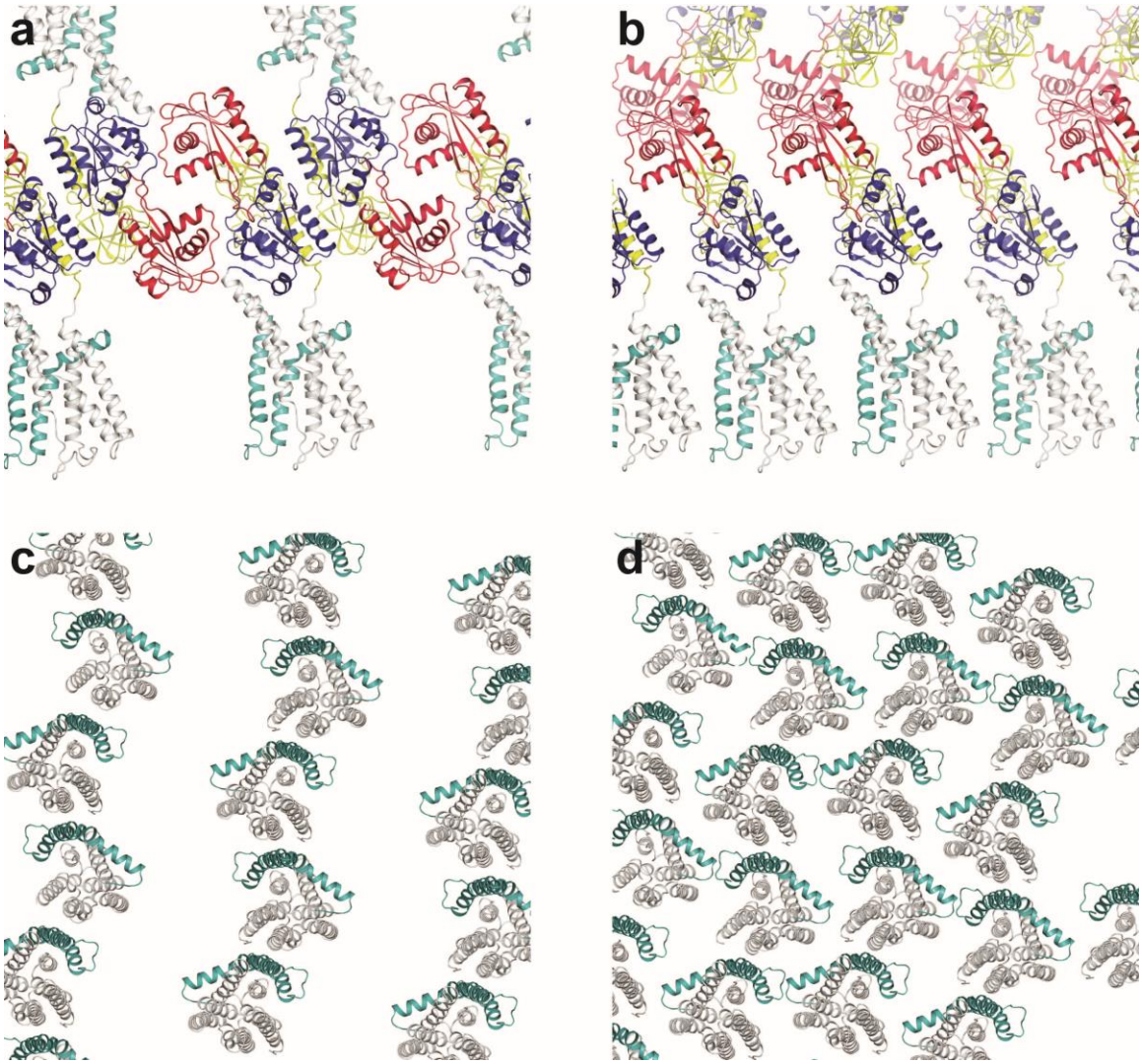

Supplementary Figure 6. Crystal packing of the two different E2P crystal forms of LpCopA. The domains are colored as in Fig. 1a. The proteins are arranged as stacked bilayers, held together by hydrophobic interactions between their membrane-spanning regions typical of the HiLiDe crystallization method[3]. **a,** View along the membrane bilayer for the C2 crystal form. **b,** Equivalent view for the $P2_12_12_1$ crystal form. Approximate perpendicular views are of panels a and b are shown in **c** and **d**, respectively. Note the more loose packing of the C2 lattice. The unit cell parameters can be found in Table 1.

Figures – Supplementary Figure 7

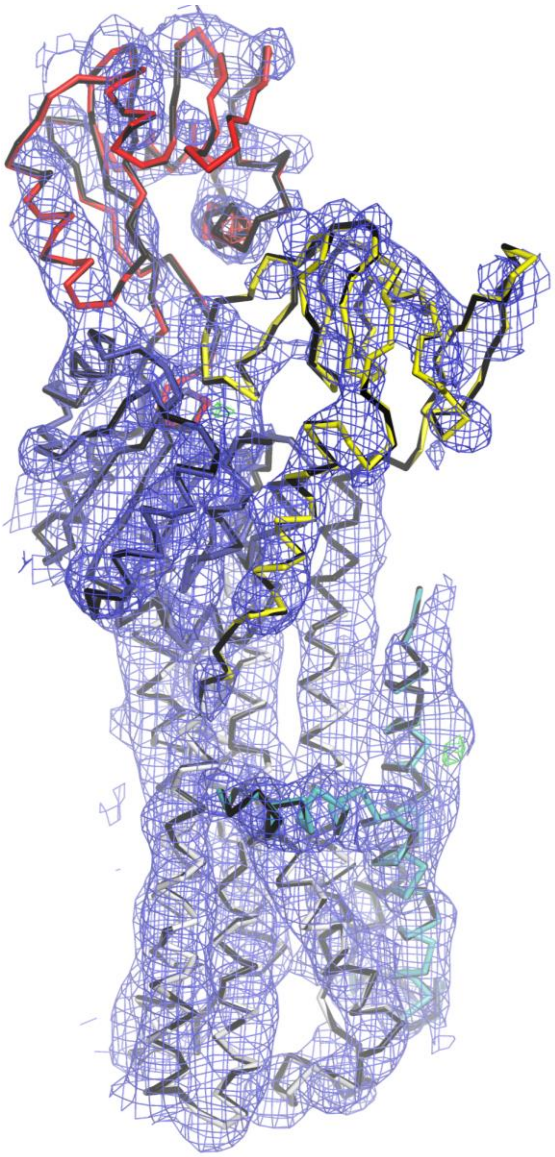

Supplementary Figure 7. Electron density maps of the low-resolution E2P structure in the second crystal form. The low- (colored as in Fig. 1a) and high-resolution (black) E2P structures overlayed. The 2mFo-DFc (blue, σ=1) and mFo-DFc (green and red, σ=4) electron density maps after rigid body refinement display no major deviation from the high-resolution model (in support that the E2P and E2.P_i states of CopA are similar in contrast to the equivalent states of SERCA). Both maps are carved around 3 Å of the molecule.

Figures – Supplementary Figure 8

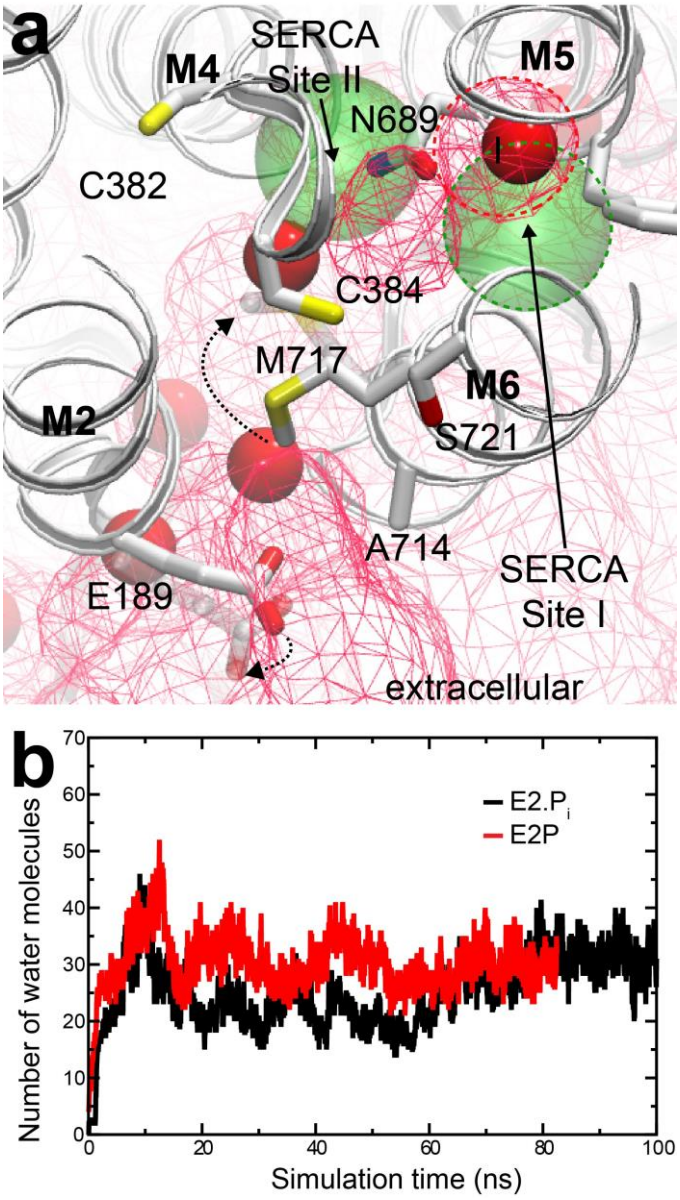

Supplementary Figure 8. Copper transfer from the high-affinity binding sites and extracellular release via Glu189. a, View from intracellular side of the E2P simulation. See Fig. 4 for details. **b,** Number of water molecules associated with the release pathway in the E2P and E2.P_i simulations.

Figures – Supplementary Figure 9

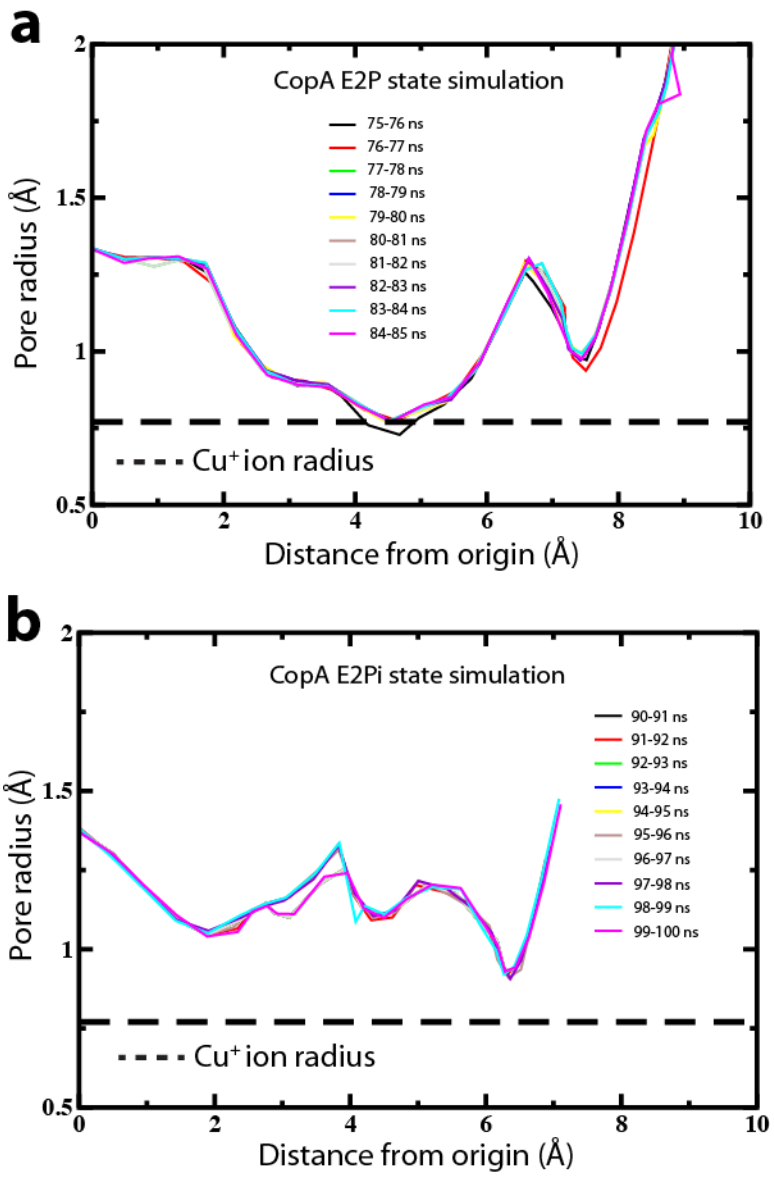

Supplementary Figure 9. Radius analyses extracted from the MD simulations. a, To determine the structural variations of the release pathway within the 10 ns average from the MD simulations presented in Fig. 3c, the last 10 ns of the E2P (**a**) and E2.P_i (**b**) simulations were divided into 10 equally spaced 100 ps averages and subjected to Caver analyses (see Supplementary Fig. 10 for details). The simulated structures were both more opened towards the extracellular side, which is consistent with the observed shifts

of the extracellular ends of TM helices MA and M6. To enable a comparison to the LpCopA crystal structures, hydrogens were stripped from average structures from the LpCopA simulations. Furthermore, the non-stripped simulated structures also had conduits with wider radii throughout than Cu^{+}.

Figures – Supplementary Figure 10

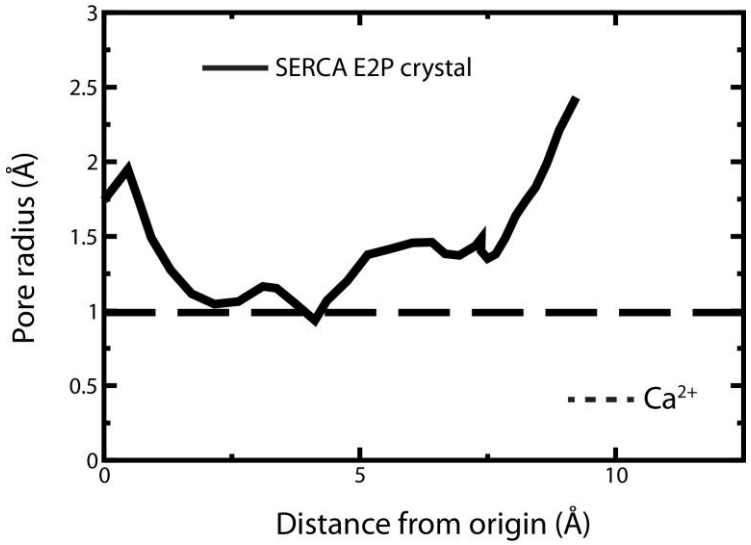

Supplementary Figure 10. Radius analysis of the corresponding E2.P_i (pdb-id: 3B9R) and E2P (pdb-id: 3B9B) SERCA states. The software CAVER[4] was used to calculate the pore radii as a function of distance from an origin. The cut-off value for all analyses was set at a pore radius of 2.5 Å. For SERCA, the origin was set close to the internal ion-binding sites, defined by the center-of-mass of Ile307, Glu309 and Leu797. While the E2P structure was open and resulted in the plotted pore radius, the E2.P_i state was closed and no pore was found.

Figures – Supplementary Figure 11

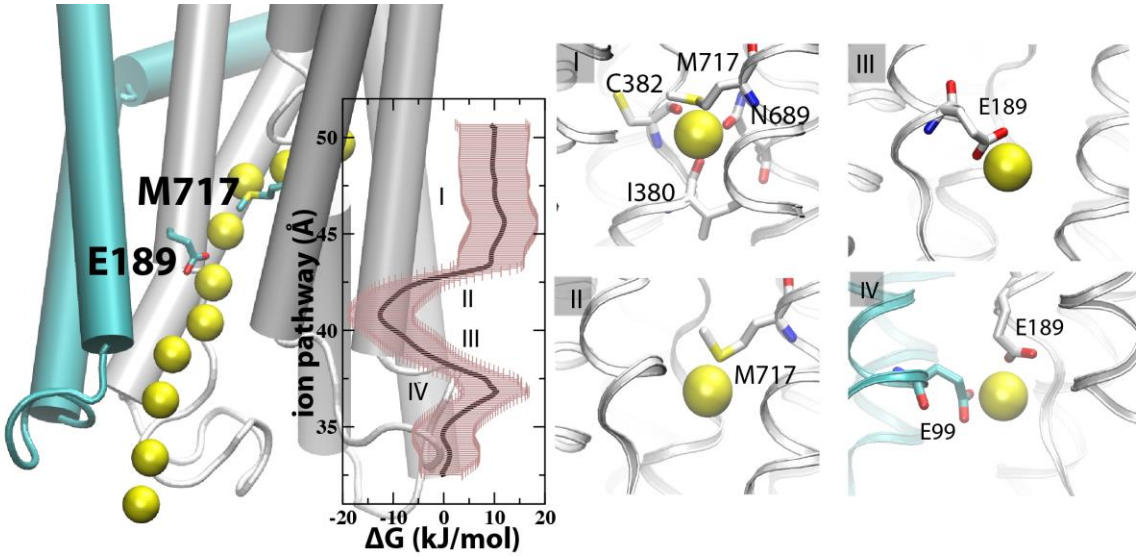

Supplementary Figure 11. Energy barriers associated with the release pathway. The release pathway as sampled by applying a force to a Cu^{+} ion initially placed in the suggested ion-binding site at z= 52 Å is displayed by snapshots of the ion during the steered MD simulation (yellow spheres). The accompanying potential of mean force (PMF), with error bars, for the sampled path is shown in the inset. Panels I-IV show the immediate protein interactions of the ion at specific parts of the release pathway. Cyan-colored helices are class-specific, while common helices are shown in white (see Supplementary Methods for details on the PMF calculation).

Figures – Supplementary Figure 12

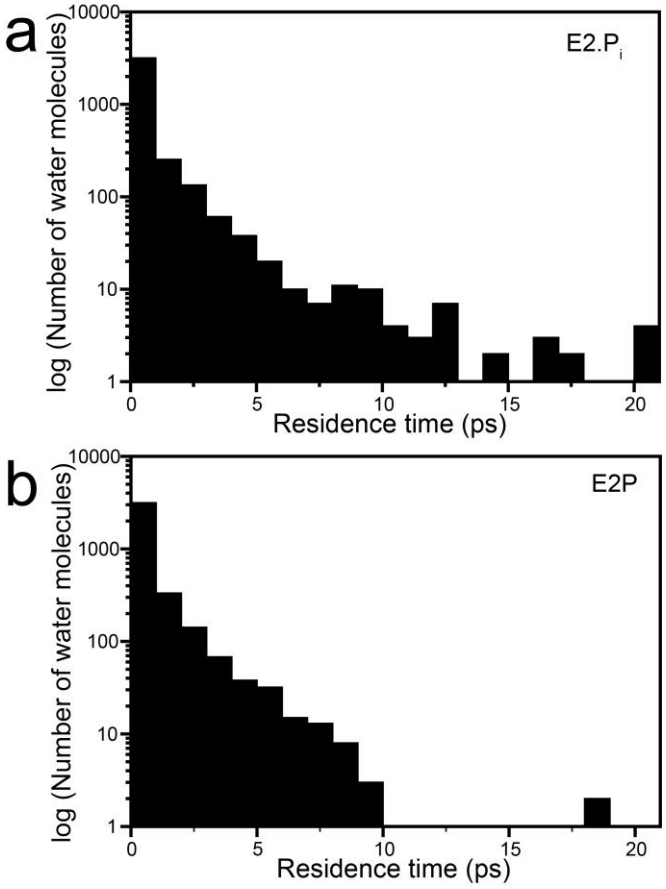

Supplementary Figure 12. Residence times for water molecules associated with the release pathway in the E2.P$_i$ (A) and E2P (B) simulations. Water within 7 Å of Glu189 were observed to cover the proposed release pathway and were therefore used to define the boundaries in the calculation of the residency times. Two crystal waters remain associated with the internal water pockets within the release pathway for the entire E2P simulation and hence have residency times of 85 ns (not included in plot 11b).

Figures – Supplementary Figure 13

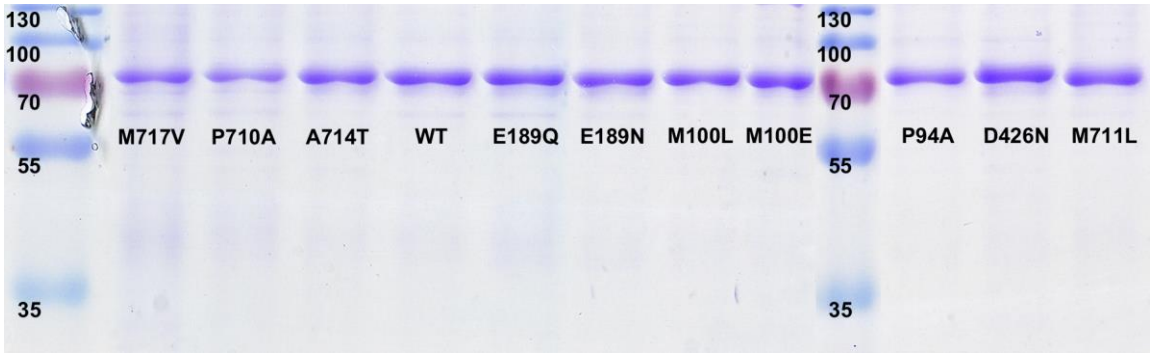

Supplementary Figure 13. Purity of the functionally assayed LpCopA constructs used for the *in vitro* assay. SDS-PAGE gels of the purified LpCopA constructs following a first round of scaling using ImageJ. Identical relative amounts of protein were used for the Baginski assay[5] for generating the raw data shown in Supplementary Table 1.

Figures – Supplementary Figure 14

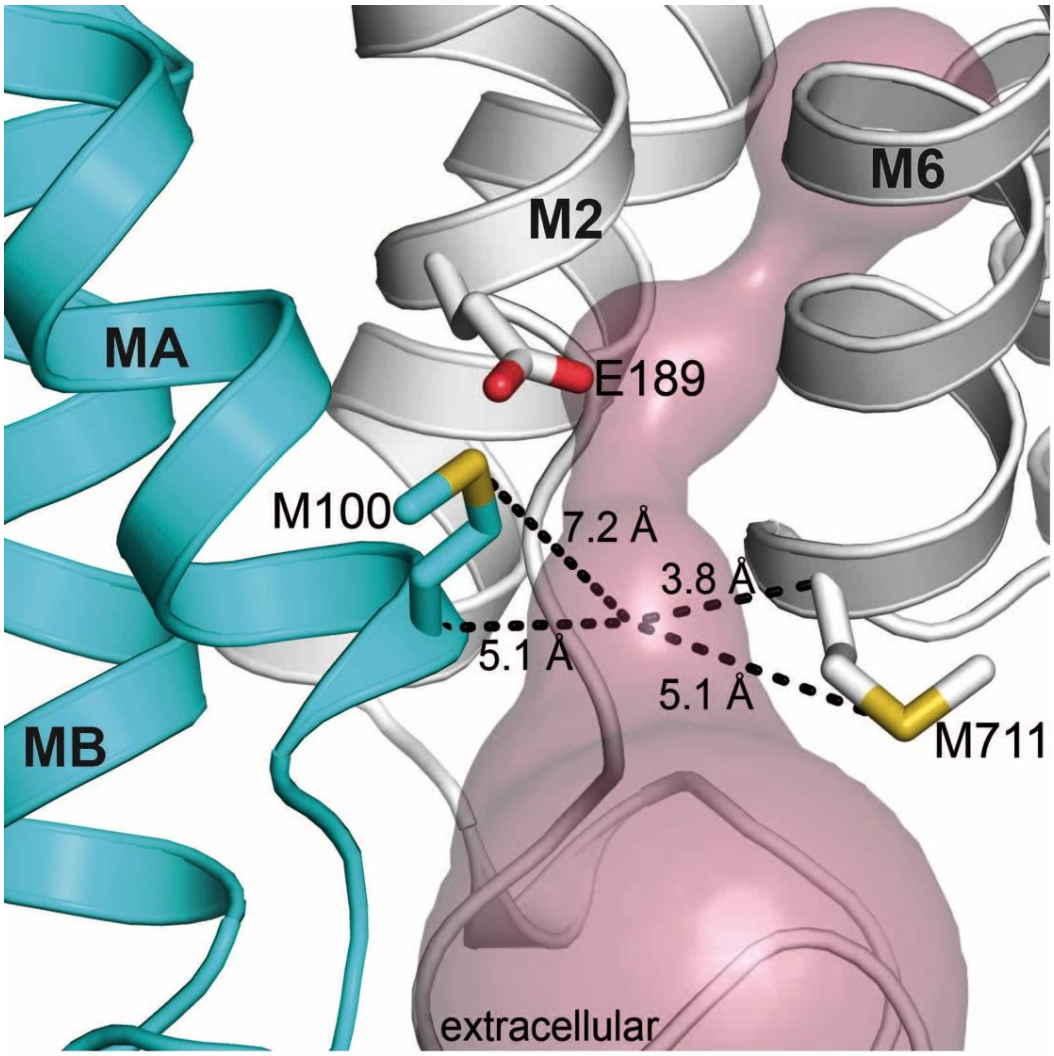

Supplementary Figure 14. Close-view of the previously suggested exit site of LpCopA involving Glu189, Met100 and Met711[2]. The E2P state of LpCopA and the extrusion pathway are shown as in Fig. 2c. The distances from the center of the extrusion pathway to the Cα and sulfur atoms of Met100 and Met711 are shown as black dotted lines. Note the peripheral location of Met100 and Met711 relative to the pathway and how the larger distances for Met100 are congruent with our mutational *in vitro* analysis (Fig. 4c).

Figures – Supplementary Figure 15

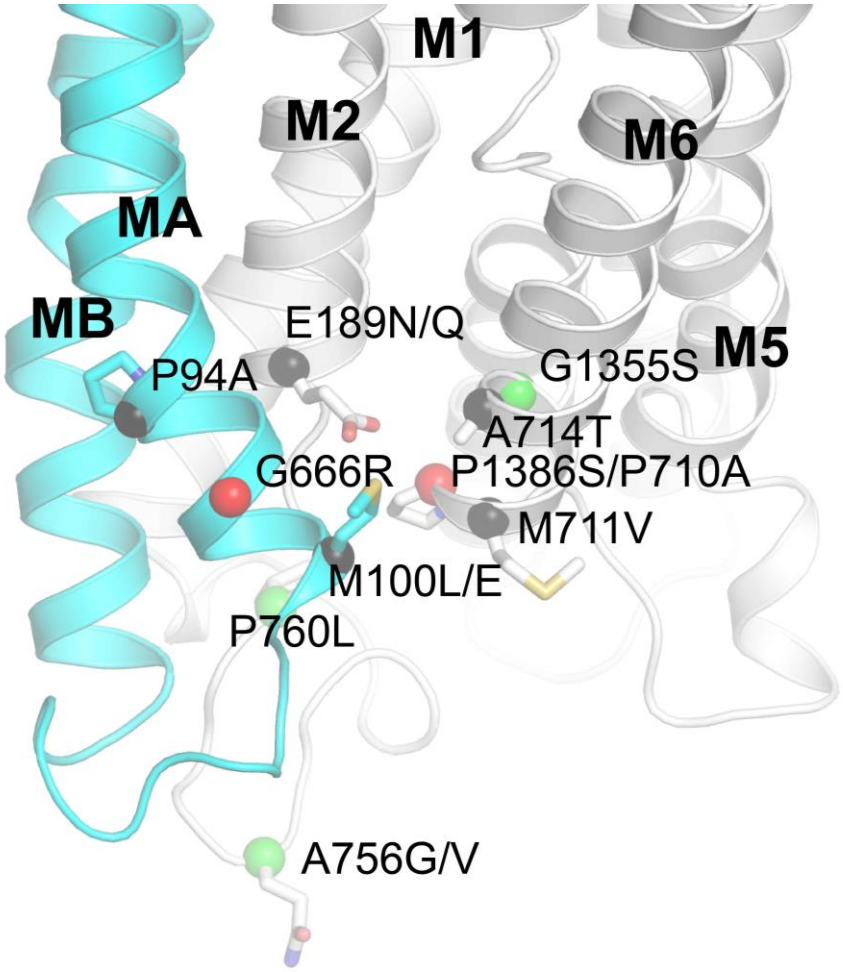

Supplementary Figure 15. Menkes' and Wilson's disease causing missense mutations in extrusion pathway region. The E2P conformation of LpCopA and the release pathway are shown as in Fig. 2c. Residues affected by disease-causing single missense mutations in Menkes' and Wilson's disorders, respectively, are depicted with red and green spheres, while residues pinpointed by our mutational analysis (Fig. 4c) are shown with black spheres.

Figures – Supplementary Figure 16

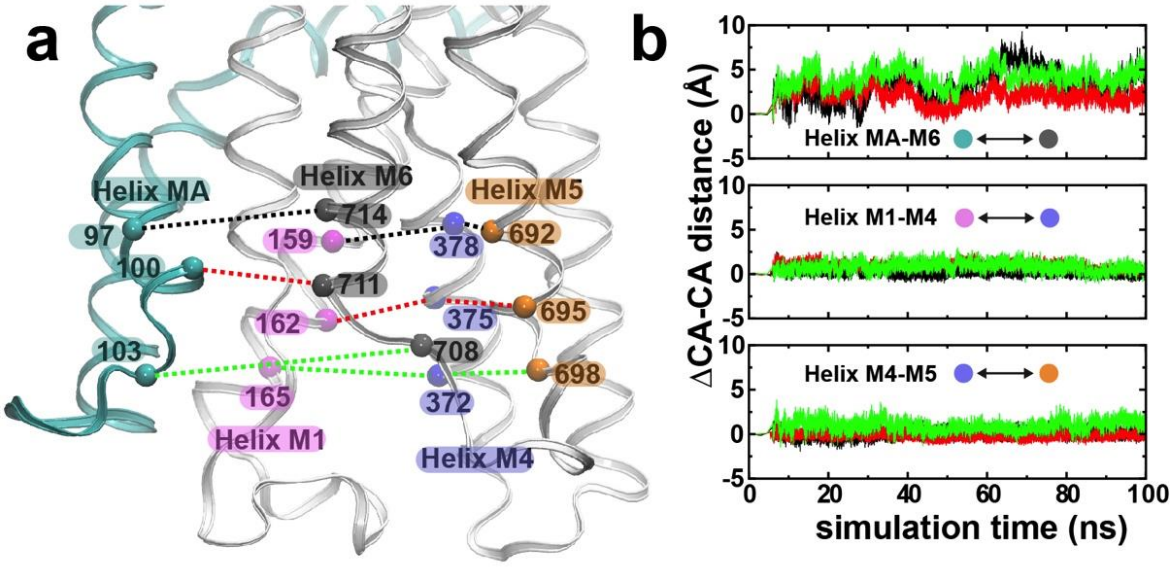

Supplementary Figure 16. Configurational dynamics at the extracellular side in the E2.P$_i$ MD simulation. a, Calculated inter-helical distances during the course of the simulation. The Cα-to-Cα distances are shown on the E2.P$_i$ structure of LpCopA structure colored as in Fig. 1a, with spheres indicating the Cα atoms from MA, M1, M4, M5 and M6 in cyan, pink, blue, orange and black, respectively. Three equally interspersed distances (along the normal to the membrane) in the transmembrane (TM) domain were measured for each TM helix pair; black (intracellular end), red and green (extracellular end) dotted lines between helices MA:M6, M1:M4 and M4:M5. See panel b for the results. **b,** Time-evolution of the inter-helical distances shown in panel a, MA:M6 (upper panel), M1:M4 (middle panel) and M4:M5 (lower panel) shown as black (intracellular end), red and green (extracellular end) lines as also shown in panel a.

Figures – Supplementary Figure 17

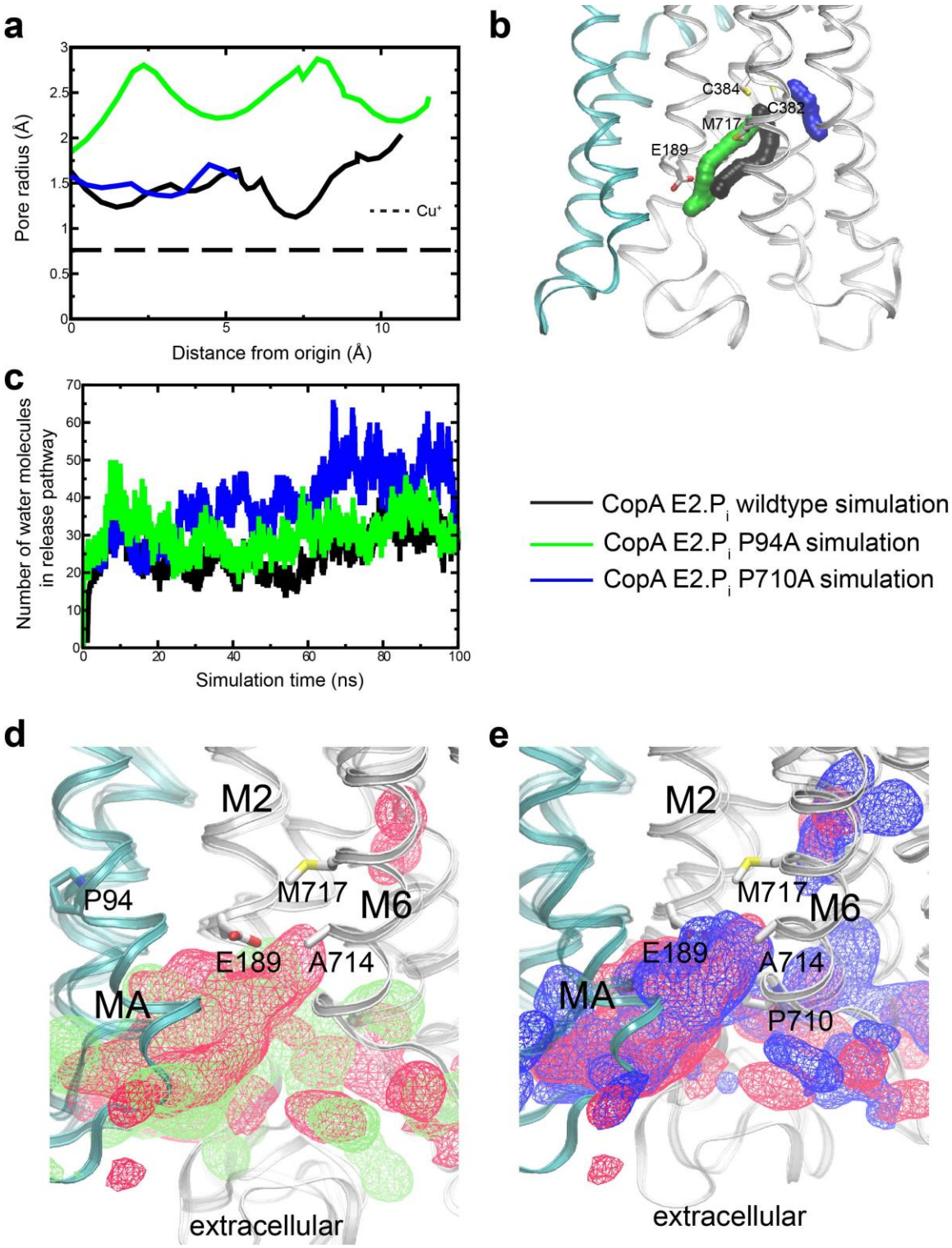

Supplementary Figure 17. Altered hydration patterns for the E2.P_i simulations of the Pro94Ala and Pro710Ala mutants of LpCopA support the proposed proline-dependent opening mechanism. a, Pore radius analyses of average structures from the E2.P_i simulations; wild-type, Pro94Aal and Pro710Ala. **b,** Structural representation of the pores predicted by Caver. **c,** Number of water molecules associated with the release pathway in the E2.P_i simulations; wild-type, Pro94Ala and Pro710Ala. **d,** Average representations from the simulations of wild-type LpCopA (full) and the Pro94Ala mutant (transparent) with the proteins colored as in Fig. 1a, with the sidechains of Pro94, Met717 and Glu189 pinpointed. Water is shown as red (wild-type) and green (mutant) iso-density surfaces at 22 % occupancy (indicating the presence of water in 22 % of the simulation frames). Note how less water enters the transmembrane domain of the Pro94Ala mutant. **e,** Average representations from the simulations of wild-type LpCopA (full) and the Pro710Ala mutant (transparent) with the proteins colored as in Fig. 1a, with the sidechains of Glu189, Met717 and Pro710 pinpointed. Water is shown as red (wild-type) and blue (mutant) iso-density surfaces at 22 % occupancy (indicating the presence of water in 22 % of the simulation frames). Note the increased water solvation compared to wild-type.

Figures – Supplementary Figure 18

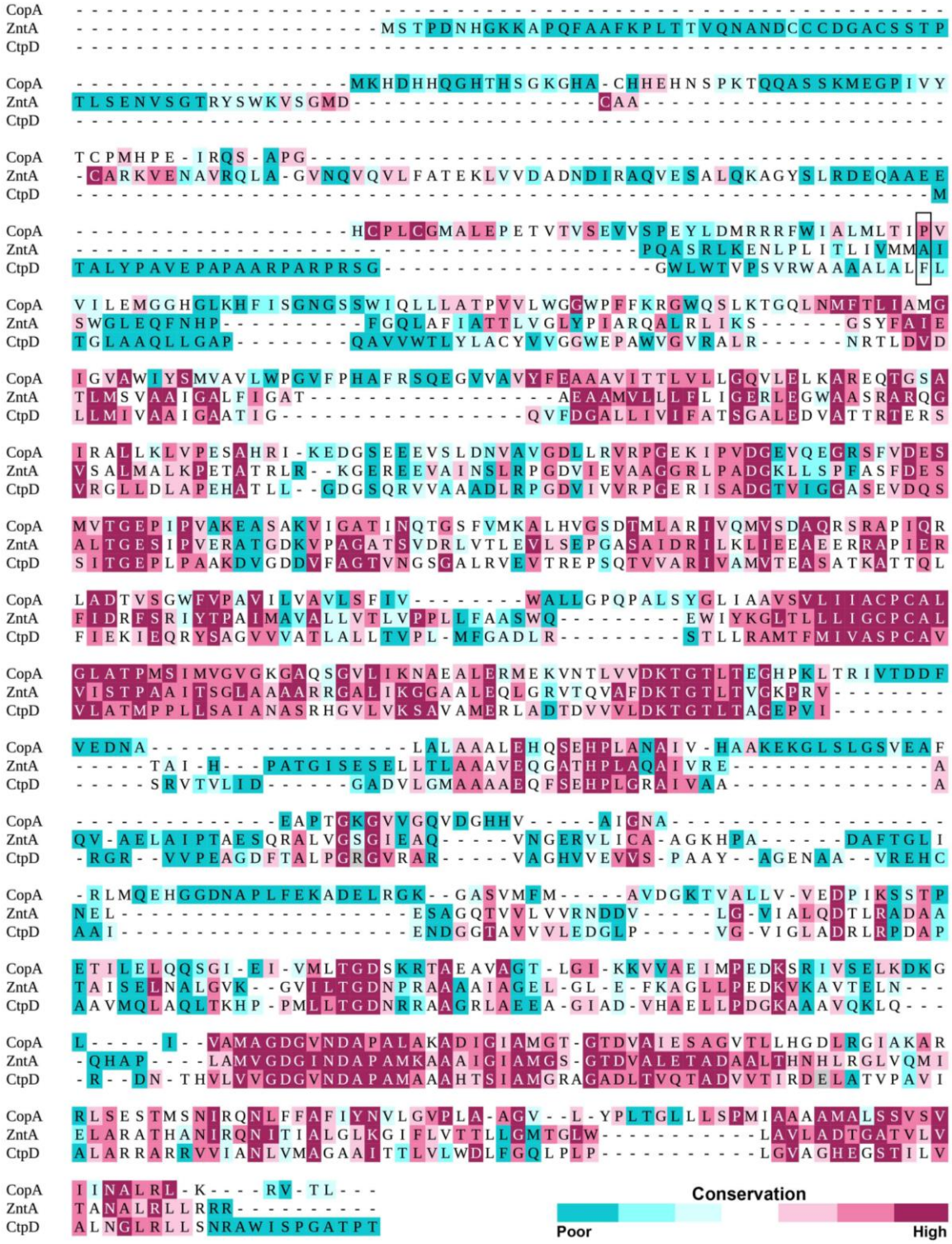

Supplementary Figure 18. Alignment and sequence conservation of representative members of the P_{IB-1}-, P_{IB-2}- and P_{IB-4}-ATPases. The sequences used have locus tags

Lpg1024 (CopA), JW3434 (ZntA) and msmeg_5403 (CtpD). For analysis of conservation level, the ConSurf server was used[6]. Determination of conservation was based on 617 sequences having a sequence identity below 95% for P_{IB-1}-ATPases, 520 sequences below identity=99% for P_{IB-2}-ATPases and 607 sequences below identity=99% for P_{IB-4}-ATPases. Information from Supplementary Fig. 22 was used for adjusting the alignments of helices MA and MB due to poor sequence conservation in this region. The black box indicates the position of Pro94 in LpCopA.

Figures – Supplementary Figure 19

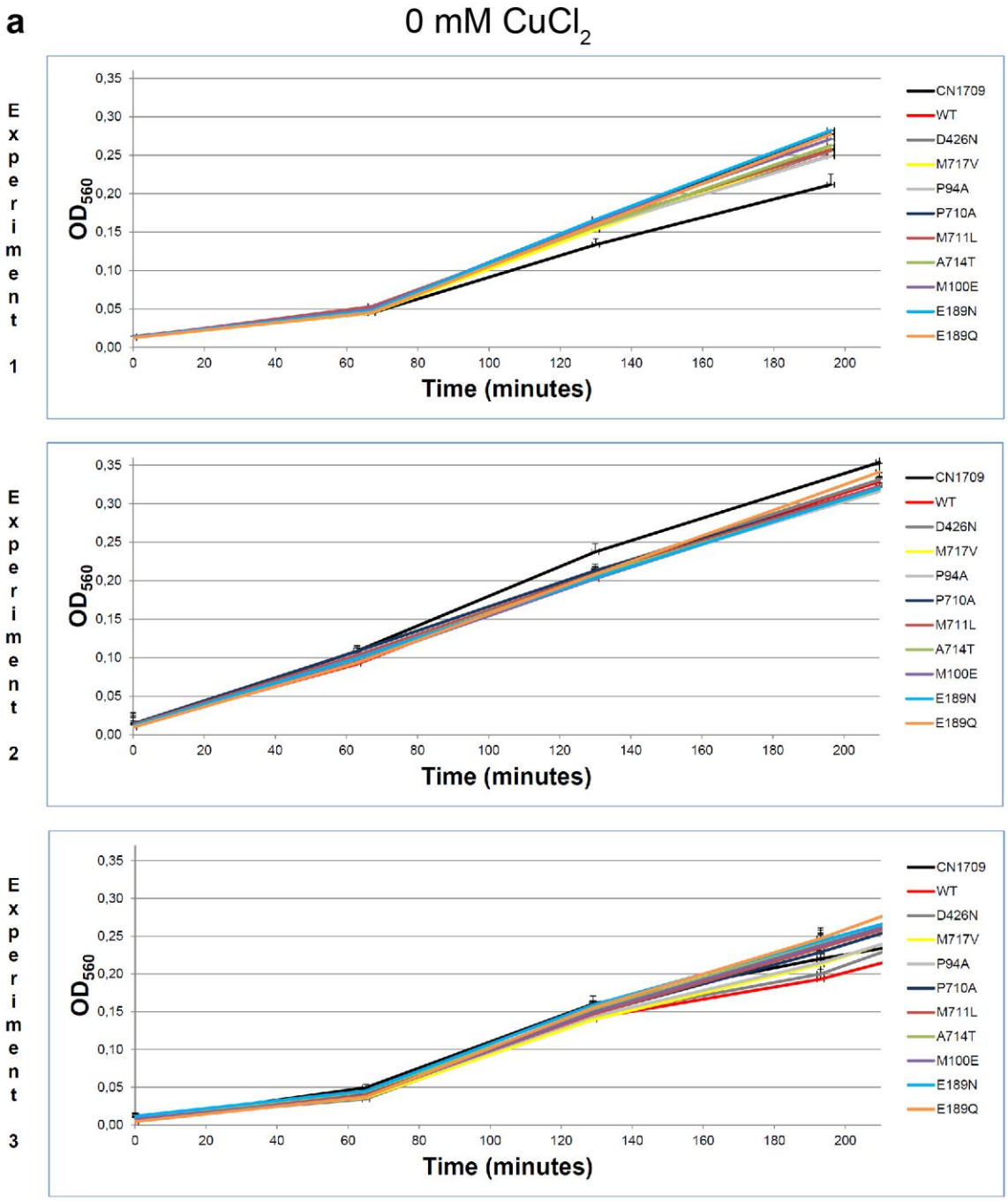

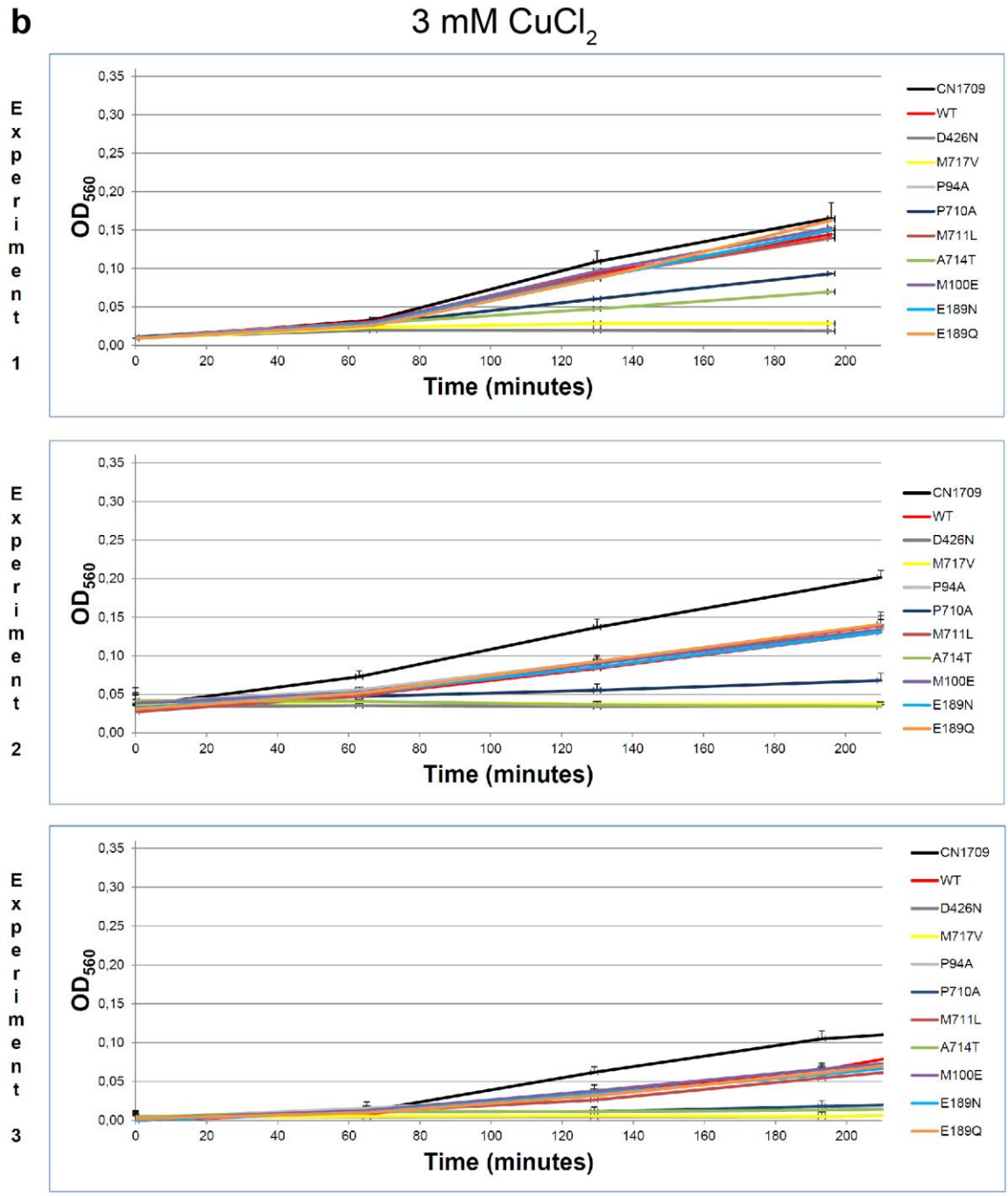

Supplementary Figure 19. The *in vivo* copper susceptibility assay. *E. coli* growth complementation curves from three independent experiments for wild-type LpCopA (WT, red), the inactive Asp426Asn mutant (gray), the high-affinity coordinator mutant Met717Val (yellow) as well as various release pathway mutants are displayed.

Experiments 1 and 3 used three replicates each, experiment 2 used 15 replicates. The assay was conducted using the CopA deleted *E. coli* strain CN2328[7] transformed with a plasmid containing the *E. coli* promotor for CopA prior to each separate LpCopA construct. The *E. coli* strain CN1709[7] with intact genomic CopA was used as a positive control (see Methods for details). **a,** 0 mM copper in the growth medium. **b,** 3 mM copper in the growth medium.

Figures – Supplementary Figure 20

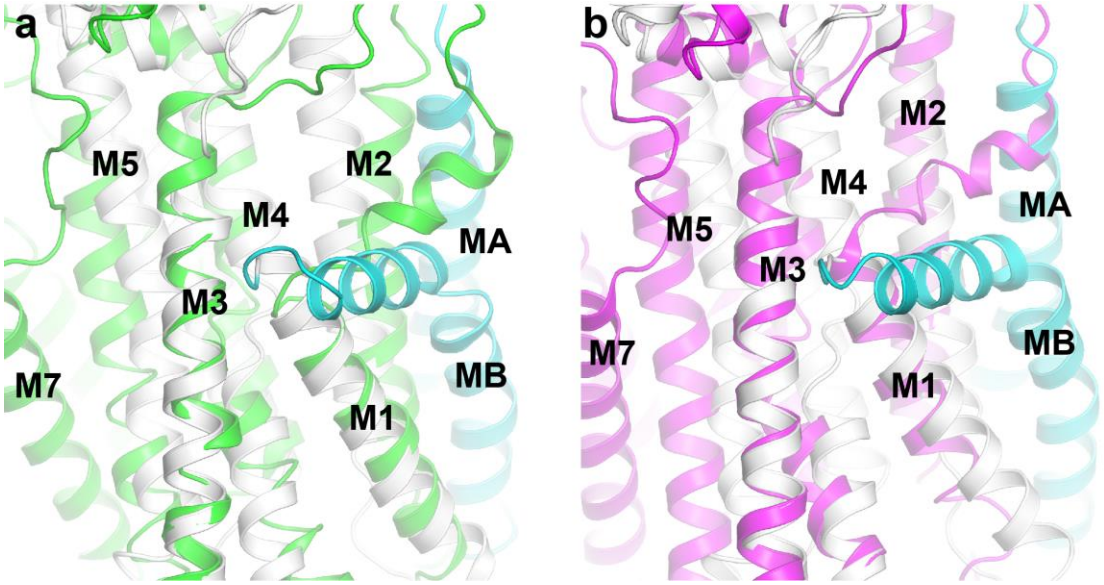

Supplementary Figure 20. Notable structural difference between SERCA and CopA that may be responsible for the decoupling of occlusion and dephosphorylation in CopA. See also Supplementary Fig. 21. **a,** The E2.P_i states of LpCopA (pdb-id: 3RFU[2]) and SERCA (pdb-id: 3B9R[1]) aligned on M3 (residues 330-357 in LpCopA and 243-279 in SERCA). The transmembrane helices are colored green for SERCA while CopA is shown in white except for MA and MB in cyan. **b,** Equivalent view as in panel a of the E2P states of CopA and SERCA (pdb-id: 3B9B[1]) (purple) aligned on M3 (residues 330-357 in LpCopA and 243-279 in SERCA) and with CopA colored as in panel a. In SERCA the A-domain plays a key role for transmitting the conformational changes in the intracellular domains to changes in the transmembrane domain allowing closure of the open E2P state and its release pathway between M1-M2, M3-M4 and M5-M6. The closing shifts of M1 and the associated M2 are precluded in CopA (see also Supplementary Figs. 4-5) due to the missing linker to the N-terminal portion of the A-domain (see also Supplementary Fig. 1) which is replaced by MB in CopA. The tighter packing of MB to M3 in CopA relative to the linker between M1 and the A-domain to

M3 in SERCA may also prevent helices M3 and the associated M4 from contributing to closing.

Figures – Supplementary Figure 21

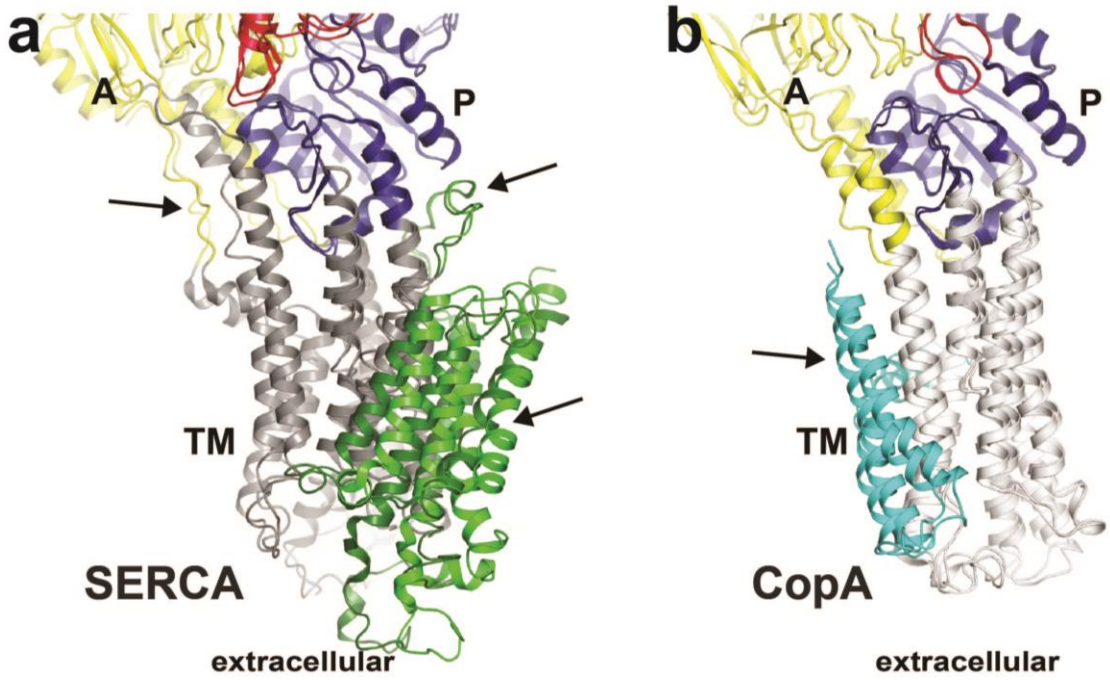

Supplementary Figure 21. Notable structural difference between SERCA and CopA that may be responsible for the decoupling of occlusion and dephosphorylation in CopA (marked by arrows). a) The E2.P_i (pdb-id: 3B9R[1]) and E2P (pdb-id: 3B9B[1]) states of SERCA aligned on the P-domain. b) Equivalent view as in panel a of the E2.P_i (pdb-id: 3RFU[2]) and E2P states of LpCopA aligned on the P-domain. The different linkers between the transmembrane (helices M4 and M5) and the P-domains, the absent connection between M1 and the A-domain replaced by MA and MB in CopA as well as the additional transmembrane helices (M7-M10) in SERCA may strongly influence how the conformational changes in the soluble domain associated with dephosphorylation are communicated and thus affect the transmembrane domains. See also Supplementary Fig. 20.

Figures – Supplementary Figure 22

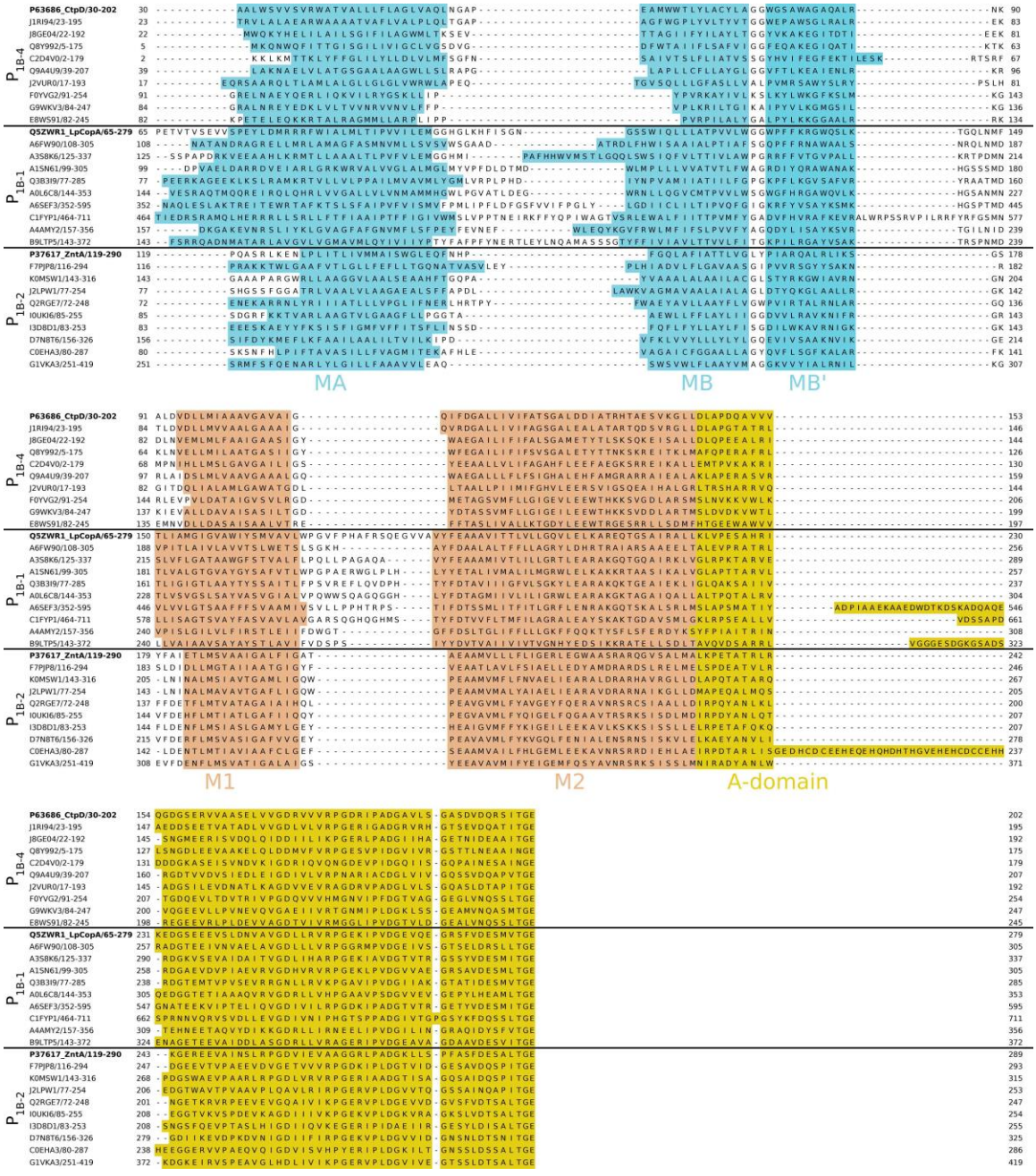

Supplementary Figure 22. Secondary structure based alignment of the N-terminal segment of the ATPase core of P_{IB-1}-, P_{IB-2}- and P_{IB-4}-ATPases. 10 weakly redundant members of each subgroup were selected and aligned based on secondary structure prediction using the PSIPRED server[8]. Only the region from the start of helix MA to the

conserved TGE motif, associated with dehosphorylation, of the A-domain is shown. The UniProtKB entries of the sequences are indicated to the left. Highlighted in bold are first sequences in each subgroup which are also used in Supplementary Figure 18.

Figures – Supplementary Figure 23

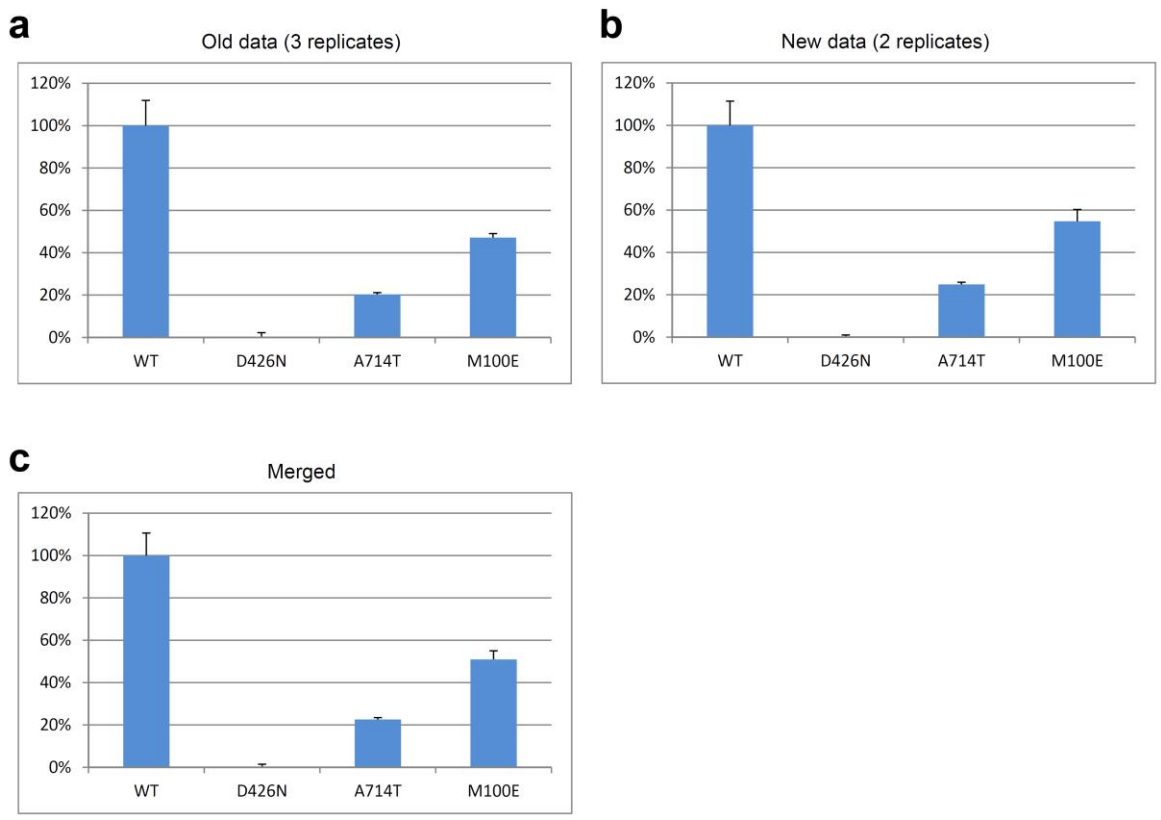

Supplementary Figure 23. Assessment of the reproducibility of the *in vitro* assay. As the *in vitro* data shown in Fig. 4c are based on a single experiment (with nine replicates, panel a), wild-type, Asp426Asn, Ala714Thr and Met100Glu LpCopA were reproduced using an additional experiment (with six replicates, panel b). The data from the two experiments are highly consistent (merged data in panel c).

Figures – Supplementary Figure 24

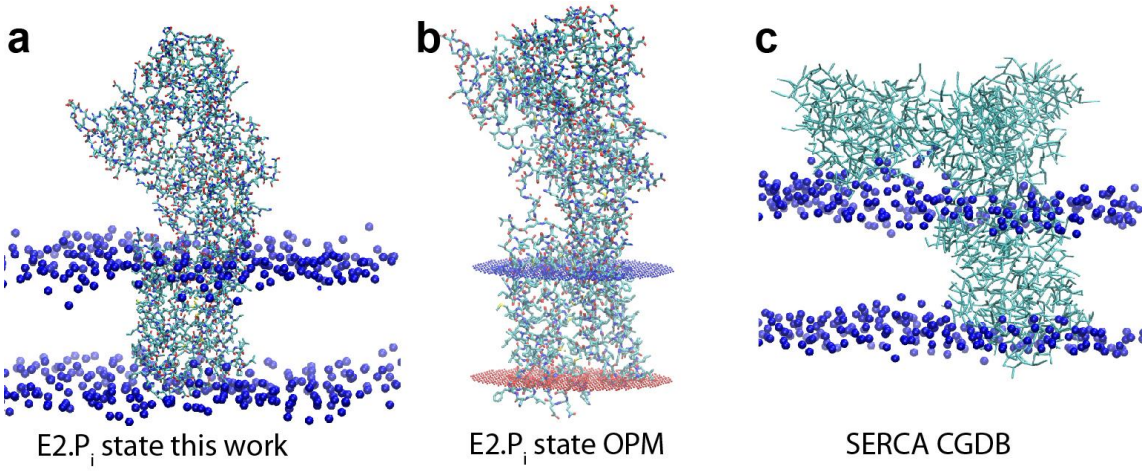

Supplementary Figure 24. Results of different protein insertion techniques. a, alignment of centers-of-mass of the TM region with the lipid bilayer. **b,** Using the "Orientations of proteins in membranes (OPM) database"[9]. **c,** Using the "Coarse-grained database" for SERCA[10].

Figures – Supplementary Figure 25

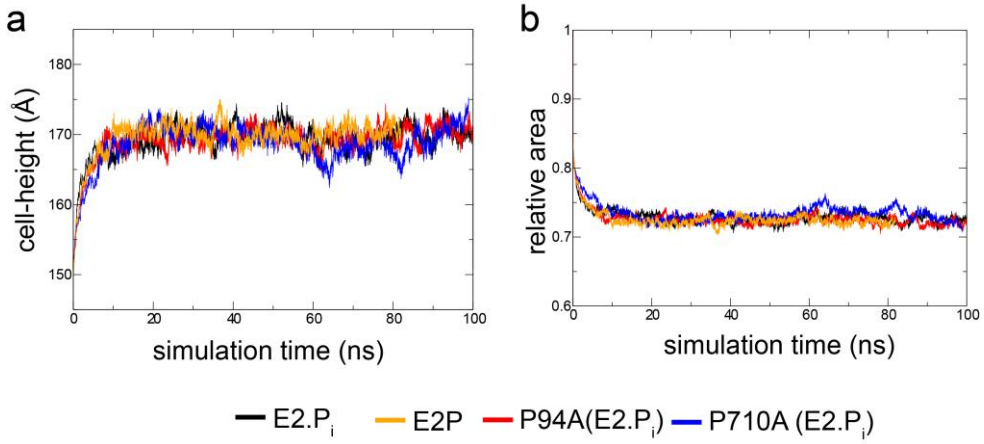

Supplementary Figure 25. Equilibration of the CopA simulations. (a) shows the evolution of the simulation box cell height over the time-course of the simulation for states E2.P_i (black) and E2P (orange) and E2.P_i mutants P94A (red) and P710A (blue), while (b) shows the corresponding relative cell area (X,Y) evolution.

Figures – Supplementary Figure 26

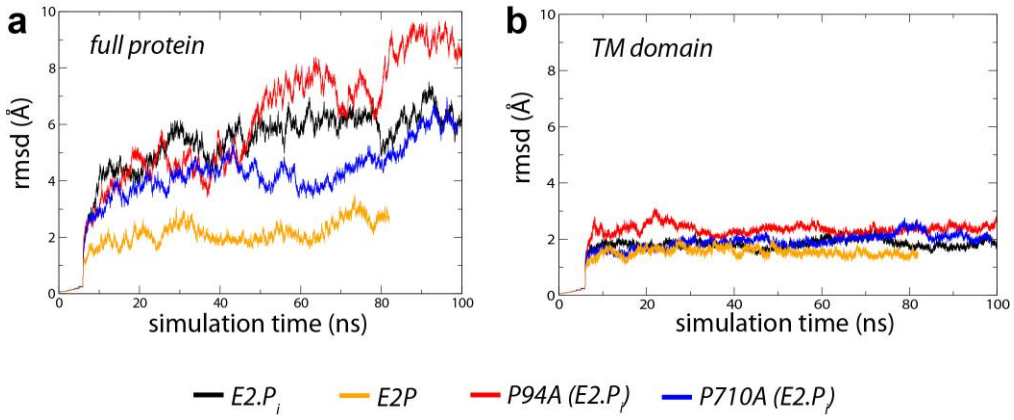

Supplementary Figure 26. RMSD measured over the MD trajectory for states E2.P_i (black) and E2P (orange) and E2.P_i mutants P94A (red) and P710A (blue) backbone atoms in the full CopA protein (a) and the transmembrane domain (b).

Figures – Supplementary Figure 27

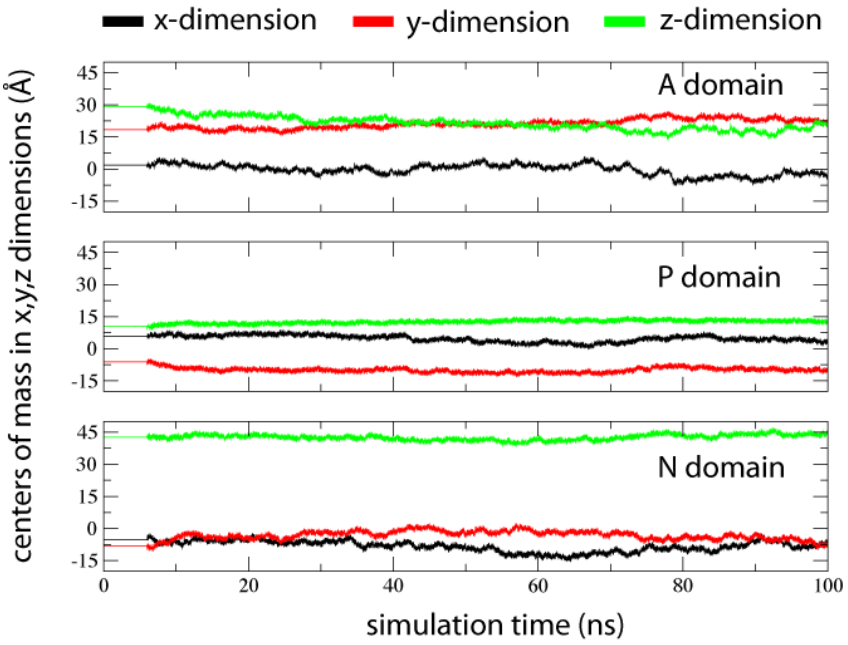

Supplementary Figure 27. Centers of mass in x (black), y (red) and z (green) dimensions of the intracellular A-, P- and N-domains over the full trajectory of the E2.P_i simulation.

Tables – Supplementary Table 1

WT	D426N	M717V	P94A	P710A	M711L	A714T	M100L	M100E	E189N	E189Q
1.483	0.393	0.358	0.615	0.355	0.637	0.492	1.130	0.743	0.564	0.805
1.466	0.389	0.357	0.603	0.351	0.631	0.498	1.141	0.700	0.568	0.817
1.308	0.362	0.322	0.582	0.338	0.565	0.474	1.020	0.729	0.533	0.732
1.479	0.393	0.342	0.615	0.337	0.642	0.503	1.121	0.758	0.533	0.886
1.395	0.388	0.360	0.596	0.342	0.662	0.507	1.155	0.768	0.540	0.921
1.588	0.368	0.319	0.632	0.329	0.626	0.501	1.080	0.758	0.519	0.874
1.649	0.336	0.330	0.588	0.315	0.598	0.481	1.148	0.784	0.564	0.942
1.659	0.373	0.340	0.588	0.317	0.599	0.496	1.148	0.752	0.557	0.910
1.708	0.338	0.322	0.534	0.291	0.547	0.480	1.100	0.770	0.511	0.796
Averages:										
1.526	0.371	0.339	0.595	0.331	0.612	0.492	1.116	0.751	0.543	0.854
Scaled between WT (100%) and D426N (0%):										
100%	0%	-3%	19%	-4%	21%	11%	64%	33%	15%	42%

Supplementary Table 1. **Raw data from the activity measurements of the different LpCopA constructs used to estimate their ATPase activities.** The absorbance was measured at 860 nm and is color-coded from green to red (strong to weak). Below the table the averaged values have been calculated and, finally, the scaled data where the background, the absorbance measured for the D426N dead mutant, has been removed and then divided with the average absorbance for the wild-type (WT).

Tables – Supplementary Table 2

WT	D426N	M717V	P94A	P710A	M711L	A714T	M100L	M100E	E189N	E189Q
Integrated band intensities:										
7722675	8637304	5480970	6723758	4578525	7638705	6626940	6654735	6480825	6877605	7787190
Signal scaling factor:										
0.894	1.000	0.635	0.778	0.530	0.884	0.767	0.770	0.750	0.796	0.902
Raw averages:										
1.526	0.371	0.339	0.595	0.331	0.612	0.492	1.116	0.751	0.543	0.854
Scaled averages:										
1.707	0.371	0.534	0.764	0.624	0.692	0.642	1.448	1.001	0.682	0.947
Scaled between WT (100 %) and D426N (0 %), based on scaled averages:										
100 %	0 %	12 %	29 %	19 %	24 %	20 %	81 %	47 %	23 %	43 %

Supplementary Table 2. Process for obtaining the final, scaled, data displayed in Fig. 4c. The LpCopA bands (at ~ 75 kDa) from the SDS-PAGE (Supplementary Fig. 13) were quantified using ImageJ by calculating their integrated band intensities. This allowed a scaling factor to be derived, by which the raw absorbance signal averages were divided, in order to obtain the scaled absorbance averages. The final scaled data was achieved by removing the background, the absorbance measured for the D426N dead mutant, and then divide the resulting background compensated values with the average absorbance for the wild-type (WT).

Methods

Figures. All structural figures in the main text were made using VMD[11], except for Fig. 2 which was done using PYMOL (www.pymol.org).

MD simulation (continued). To describe the energy barriers involved in transport of Cu^+ along the water-filled pathway, the potential of mean force (PMF) was calculated using GROMACS 4.6.3[12] and the ffGromos53a6 force field[13], which contains Cu^+ parameters. The last frame of CHARMM trajectory of the E2Pi simulation was formatted according to Gromos and a Cu^+ ion was placed between ion-coordinating residues Cys382 and Met717 to calculate the energetics involved with ion extrusion. The DOPC lipids and water molecules were described by published parameters derived from the ffGromos53a6 force field[14] and the simple point charge (SPC) water model[15], respectively. The system was first energy minimized according to a steepest descent algorithm for 5,000 steps. The GROMACS pull code was used to generate configurations for the umbrella sampling with a 1000 kJ mol^{-1} nm^{-2} force constant applied on Cu^+ in the z-dimension directed towards the extracellular side. A pull rate of 2.5 Å/ns was applied for 10 ns. The Ca's of 6 remote residues (111, 115, 169, 367, 706, 709) were restrained to keep the system from drifting when applying the force. A 2 fs time-step was used and short-range non-bonded interactions were cut off at 1.4 nm, with long-range electrostatics calculated using the particle mesh Ewald (PME) algorithm[16,17]. The temperature of the system was maintained by independently coupling the protein and non-protein atoms to an external temperature bath at 310 K using a Nose-Hoover thermostat[18,19], and the Parrinello-Rahman barostat[20,21] was used to isotropically regulate pressure. The length of all bonds within the

protein was constrained using the LINCS algorithm[22]. Snapshots spaced by 1 Å were taken from the pulling simulation to generate the starting configurations for the umbrella sampling windows. Each window was equilibrated for 100 ps followed by 5 ns of umbrella sampling followed by extraction of the PMF using the Weighted Histogram Analysis Method[23], which is implemented in the GROMACS package[24]. Statistical errors were quantified by bootstrap analysis[24].

References

1 Olesen, C. *et al.* The structural basis of calcium transport by the calcium pump. *Nature* **450**, 1036-1042 (2007).

2 Gourdon, P. *et al.* Crystal structure of a copper-transporting PIB-type ATPase. *Nature* **475**, 59-64 (2011).

3 Gourdon, P. *et al.* HiLiDe—Systematic Approach to Membrane Protein Crystallization in Lipid and Detergent. *Crystal Growth & Design* **11**, 2098-2106 (2011).

4 Petrek, M. *et al.* CAVER: a new tool to explore routes from protein clefts, pockets and cavities. *BMC Bioinformatics* **7**, 316 (2006).

5 Baginski, E. S., Foa, P. P. & Zak, B. Microdetermination of inorganic phosphate, phospholipids, and total phosphate in biologic materials. *Clin Chem* **13**, 326-332 (1967).

6 Ashkenazy, H., Erez, E., Martz, E., Pupko, T. & Ben-Tal, N. ConSurf 2010: calculating evolutionary conservation in sequence and structure of proteins and nucleic acids. *Nucleic Acids Res* **38**, W529-533 (2010).

7 Petersen, C. & Moller, L. B. Control of copper homeostasis in Escherichia coli by a P-type ATPase, CopA, and a MerR-like transcriptional activator, CopR. *Gene* **261**, 289-298 (2000).

8 Buchan, D. W. *et al.* Protein annotation and modelling servers at University College London. *Nucleic Acids Res* **38**, W563-568 (2010).

9 Lomize, M. A., Lomize, A. L., Pogozheva, I. D. & Mosberg, H. I. OPM: orientations of proteins in membranes database. *Bioinformatics* **22**, 623-625 (2006).

10 Sansom, M. S., Scott, K. A. & Bond, P. J. Coarse-grained simulation: a high-throughput computational approach to membrane proteins. *Biochem Soc Trans* **36**, 27-32 (2008).

11 Humphrey, W., Dalke, A. & Schulten, K. VMD: Visual molecular dynamics. *J Mol Graph Model* **14**, 33-38 (1996).

12 Hess, B., Kutzner, C., van der Spoel, D. & Lindahl, E. GROMACS 4: Algorithms for highly efficient, load-balanced, and scalable molecular simulation. *J Chem Theory Comput* **4**, 435-447 (2008).

13 Oostenbrink, C., Villa, A., Mark, A. E. & van Gunsteren, W. F. A biomolecular force field based on the free enthalpy of hydration and solvation: the GROMOS force-field parameter sets 53A5 and 53A6. *J Comput Chem* **25**, 1656-1676 (2004).

14 Poger, D., Van Gunsteren, W. F. & Mark, A. E. A New Force Field for Simulating Phosphatidylcholine Bilayers. *J Comput Chem* **31**, 1117-1125 (2010).

15 Berendsen, H. J. C., Postma, J. P. M., van Gunsteren, W. F. & Hermans, J. *Interaction models for water in relation to protein hydration*. 331-342 (Reidel, 1981).

16 Darden, T., York, D. & Pedersen, L. Particle Mesh Ewald - an N.Log(N) Method for Ewald Sums in Large Systems. *J Chem Phys* **98**, 10089-10092 (1993).

17 Essmann, U. *et al.* A Smooth Particle Mesh Ewald Method. *J Chem Phys* **103**, 8577-8593 (1995).

18 Hoover, W. G. Canonical Dynamics - Equilibrium Phase-Space Distributions. *Phys Rev A* **31**, 1695-1697 (1985).

19 Nose, S. A Unified Formulation of the Constant Temperature Molecular-Dynamics Methods. *J Chem Phys* **81**, 511-519 (1984).

20 Nose, S. & Klein, M. L. Constant Pressure Molecular-Dynamics for Molecular-Systems. *Mol Phys* **50**, 1055-1076 (1983).

21 Parrinello, M. & Rahman, A. Polymorphic Transitions in Single-Crystals - a New Molecular-Dynamics Method. *J Appl Phys* **52**, 7182-7190 (1981).

22 Hess, B., Bekker, H., Berendsen, H. J. C. & Fraaije, J. G. E. M. LINCS: A linear constraint solver for molecular simulations. *J Comput Chem* **18**, 1463-1472 (1997).

23 Kirkwood, J. G. Statistical mechanics of fluid mixtures. *J Chem Phys* **3**, 300-313 (1935).

24 Hub, J. S., de Groot, B. L. & van der Spoel, D. g_wham-A Free Weighted Histogram Analysis Implementation Including Robust Error and Autocorrelation Estimates. *J Chem Theory Comput* **6**, 3713-3720 (2010).